Electronic Supplementary Information: Silvanite $AuAgTe_4$ - a rare case of gold superconducting material

Yehezkel Amiel,[1] Gyanu P. Kafle,[2] Evgenia V. Komleva,[3,4] Eran Greenberg,[5,6] Stella Chariton,[6] Barbara Lavina,[6,7] Dongzhou Zhang,[6,8] Yuri S. Ponosov,[3,4] Alexander Palevski,[1] Alexey V. Ushakov,[3] Hitoshi Mori,[2] Daniel I. Khomskii,[9] Igor I. Mazin,[10] Sergey V. Streltsov,[3,4] Elena R. Margine,[2] and Gregory Kh. Rozenberg[1]

[1] *School of Physics and Astronomy, Tel Aviv University, 69978 Tel Aviv, Israel*
[2] *Department of Physics, Applied Physics, and Astronomy, Binghamton University-SUNY, Binghamton, New York 13902, USA*
[3] *M.N. Mikheev Institute of Metal Physics UB RAS, 620137, S. Kovalevskaya str. 18, Ekaterinburg, Russia*
[4] *Ural Federal University, Mira St. 19, 620002 Ekaterinburg, Russia*
[5] *Applied Physics Division, Soreq NRC, Yavne 81800, Israel*
[6] *GSECARS, University of Chicago, Chicago, Illinois 60637, USA*
[7] *X-Ray Science Division, Advanced Photon Source, Argonne National Lab, 60439, USA*
[8] *School of Ocean and Earth Science and Technology, University of Hawai'i at Manoa, Honolulu, HI 96822, USA*
[9] *II. Physikalisches Institut, Universität zu Köln, Zülpicher Straße 77, D-50937 Köln, Germany*
[10] *Department of Physics and Astronomy, George Mason University, Fairfax, USA*

(Dated: June 21, 2023)

PACS numbers:

I. EXPERIMENTAL AND CALCULATION DETAILS

Samples. The experiments on X-ray diffraction and resistance were performed with high-quality natural single-crystal of silvanite, $AuAgTe_4$, from the classical Transylvania locality from the private collection of Prof. Ladislav Bohatý and Petra Becker-Bohatý, University of Cologne.

The Raman experiment was carried out using high-quality natural single-crystals of silvanite from the Kochbulak deposit, Kuraminsky Range, Uzbekistan. Their composition and structure were confirmed using a Cameca SX100 electron probe microanalyzer and a Jeol JSM6390LV scanning electron microscope with an Inca Energy 450 X-Max80 EDS detector. For Raman single crystals the atomic composition matches well the ideal sylvanite stoichiometry: observed deviations are ∼1-2 at.%, which is within the measurement error of 3%.

Transport measurements. For our transport measurements, pressure was generated using TAU opposing-plate diamond anvil cells (DACs)[1] with diamond anvil culets of 400 μm. A pre-indented rhenium gasket was drilled and then filled and covered with a powder layer of 75% Al_2O_3 and 25% NaCl for electrical insulation. A piece of single-crystal $AuAgTe_4$ with an average size of $\sim 0.02\times0.02\times0.01$ mm^3 was placed onto the culets. A Pt foil with a thickness of 5-7 μm was cut into triangular probes connecting the sample and the copper leads, allowing electrical transport measurements at elevated pressures. 6 probes were placed in each DAC. A few ruby fragments for pressure determination[2] were located in the region between the Pt electrode tips overlapping the sample. No pressure-transmitting medium was used, but pressure is effectively transmitted to the sample upon compression by way of the surrounding Al_2O_3+NaCl insulation. The ruby spectra suggest a $\sim$ 10% pressure inhomogeneity.

Electrical transport measurements were performed in a dilution refrigerator, equipped with cryogenic radiation filters (QDevil both RF and RC) for all electrical lines, and using a physical property measurement system (PPMS Quantum Design, USA). Three slots of resistance measurements were performed (runs 1, 2, 3) up to 11.2, 4.3 and 10.8 GPa, respectively. The sample was compressed up to ∼11 GPa in increments of $\sim 0.5-1$ GPa on average, and cooled down from ambient temperature down to 0.04 K. After each pressure increment a temperature cycle was performed.

Single-crystal XRD. These experiments were performed at room temperature up to ∼11 GPa, mainly at beamline 13-ID-D of the APS synchrotron (Argonne, IL, USA), with a wavelength of $\lambda = 0.2952$ Å, and a spot size of 3(V)×4(H) μm. A single crystal of an orthoenstatite $[(Mg_{1.93},Fe_{0.06})(Si_{1.93},Al_{0.06})O_6$, space group Pca with $(a) = 18.2391(3)$, $(b) = 8.8117(2)$, and $(c) = 5.18320(10)$ Å], was used to calibrate the instrument model of CrysAlisPro (sample-to-detector distance, the detector's origin, offsets of the goniometer angles and rotation of the X-ray beam and the detector around the instrument axis). XRD wide images were collected during continuous rotation of DACs typically from –35 to +35 on omega; while XRD single-crystal data collection experiments were performed by narrow 0.5° scanning of the same omega range. Either a MARCCD 165 or a Pilatus 1M CdTe detector was used. DIOPTAS software[3] was used for preliminary analysis of the 2D images and calculation of pressure values from the positions of the XRD lines of Ne[4].

A piece of single crystal of $AuAgTe_4$ with an average size of $0.02\times0.02\times0.01$ mm^3 together with a small ruby

chip (for pressure estimation) were loaded into BX90-type DAC[5] equipped with Boehler-Almax diamonds with 300 μm culet size. Neon was used both as a pressure transmitting medium and as a pressure standard. The DAC was compressed to 10.8 GPa with steps of 2−5 GPa and then decompressed to 0.2 GPa with steps of 1 − 2.5 GPa with wide images being collected at each pressure point. The single-crystal XRD datasets were collected only at a few selected pressure points (see Table S1) in order to determine the crystal structure. The indexing of the unit cell, integration of the reflection intensities and absorption corrections were performed using CrysAlisPro software[6]. The software package JANA[7,8] was used for structure solution and refinements. When the number of reflections was sufficiently high, all atoms were refined in the anisotropic approximation, giving in total 30 and 21 refinable parameters for the P2/c and P2/m phases, respectively with typically over 300 unique reflections with $F_0 > 3\sigma(F_0)$ (see Table S2). In the few datasets that the reflection to refined parameter ratio was too low, we refined only the anisotropic parameters of the Au and Te atoms.

For pressure points at which only wide images were collected, the images were integrated using DIOPTAS, and the unit-cell parameters were determined using GSAS-II[9,10]. In these cases the sample-to-detector distance, coordinates of the beam center, tilt angle and tilt plane rotation angle of the detector images were calibrated using LaB_6 powder. Only the unit-cell parameters were refined, and a spherical harmonic model (order 4 and 2 for the $P2/m$ and $P2/c$ phases, respectively) for preferred orientation was used for properly refining the intensities (the atomic positions were fixed according to the single-crystal data for each phase). The obtained unit-cell volumes were fit to an equation of state (EOS) using EoSFit7-GUI[11].

At the highest pressure point, one single-crystal XRD measurement was carried out at beamline 13-BM-C[12] with a wavelength of $\lambda = 0.434$ Å, and a spot size of 18(V)×12(H) μm^2 FWHM, and using a Pilatus 3 1M area detector. Data was collected in the range of ±35.5°, and a diffraction scan with 0.25° step size along the ϕ-axis was completed in the full DAC opening angle to collect the diffraction images. Two detector positions ($2\theta = 0°$ and 20°) were used in the data collection. The diffraction images were reduced by the APEX3 software (Bruker). The absorption correction was carried out empirically using the SADABS package integrated to APEX3. The structure solution and refinement were carried out by SHELX package interfaced by OLEX2[13]. In total 228 independent diffraction peaks were harvested to solve and refine the structure, and the final refinement gave an R1 of 15.38% (all peaks) and a goodness of fitting of 1.157.

Raman spectroscopy. For the high pressure experiments, nonoriented crystal chips were loaded into a home-made DAC using KCl as a pressure medium together with a small ruby chip for pressure control. The polarized Raman measurements were performed in backscattering geometry using a RM1000 Renishaw microspectrometer equipped with 532 nm solid-state laser and 633 helium-neon laser. A low-power laser radiation (up to 3 mW) was used to prevent the local heating of the samples. The spectral resolution was about 2-3 cm^{-1}. Three high pressure Raman experiments were performed with the highest pressure being 7.6 GPa. Results for the higher-pressure experiments will be published elsewhere[14]. Although the orientation of the crystal plane in each of them was unknown, the results of all three measurements are in good agreement since the spectra with different sample orientations are dominated by intense fully symmetrical lines.

DFT. The Quantum Espresso (QE)[15] code was used to perform first-principles calculations within the density functional theory (DFT). We employed optimized norm-conserving Vanderbilt (ONCV) pseudopotentials[16] with the Perdew-Burke-Ernzerhof (PBE) exchange-correlation functional in the generalized gradient approximation[17]. The Brillouin-zone (BZ) integration was performed using a plane wave kinetic-energy cutoff value of 60 Ry, a Methfessel-Paxton smearing[18] value of 0.01 Ry, and a Γ-centered Monkhorst-Pack[19] **k**-mesh of 8 × 12 × 4 for the low pressure (LP) phase and 12 × 12 × 8 for high pressure (HP) phase. The dynamical matrices and linear variation of the self-consistent potential were computed using density-functional perturbation theory (DFPT)[20] on the irreducible set of a regular 4 × 6 × 2 **q**-mesh for the LP phase and 4 × 4 × 2 **q**-mesh for the HP phase.

The superconducting properties were investigated using the EPW code[21–23]. The Wannier-Fourier interpolation[24,25] was performed using forty-four maximally localized Wannier functions (d orbitals of Au and Ag atoms, and p orbitals of Te atoms) on a uniform Γ-centered 8×12×4 **k**-grid for the LP phase and twenty-two Wannier functions (d orbitals of Au and Ag atoms, and p orbitals of Te atoms) on a uniform Γ-centered 8 × 8 × 4 **k**-grid for the HP phase. The superconductivity calculations were performed using uniform 40 × 80 × 20 **k**-point and 20×40×10 **q**-point grids for the LP phase and 80×80×40 **k**-point and 40 × 40 × 20 **q**-point grids for the HP phase. When solving the isotropic Migdal-Eliashberg equations, the Matsubara frequency cutoff was set to 0.25 eV, and the Dirac deltas were replaced with Gaussians of width 25 meV (electrons) and 0.05 meV (phonons). To calculate the anisotropic superconducting gap, we used a scale parameter, $\Lambda = 10^4$ instead of the Matsubara frequency cutoff, where Λ is a cutoff used when constructing the intermediate representation basis[26–28].

II. RAMAN SPECTROSCOPY RESULTS

For the ambient pressure structure of $AuAgTe_4$ ($P2/c$ space group), group theory predicts 36 phonon modes ($10A_u + 7A_g + 11B_u + 8B_g$), out of which fifteen modes ($7A_g + 8B_g$) are Raman active. At room temperature we observe almost all Raman active vibrations: seven A_g

phonon modes at 47, 61, 95, 102, 121, 132, 158 cm^{-1} on the *ac* plane and 7 more weak B_g modes at 50, 58, 84, 88, 114, 134, 147 cm^{-1} which are observed on other crystal planes. All 15 Raman active modes are located in the 100 cm^{-1} range, which sometimes leads to lines overlapping. Nevertheless, most of the modes can be accurately identified.

Strong changes in the polarized spectra in Fig. S3 (the appearance of new lines and a change in the intensities of conserved modes) indicate a change in the crystal structure occurring in the pressure range of 4–6 GPa, as predicted. In addition to the appearance of new lines in the spectrum, the frequencies of a number of lines either increase significantly (61, 133 and 158 cm^{-1}) or decrease (147 cm^{-1}) with increasing pressure, the energies of others change nonmonotonically (102 cm^{-1}) or increase insignificantly (47 and 121 cm^{-1}) (Fig. S4).

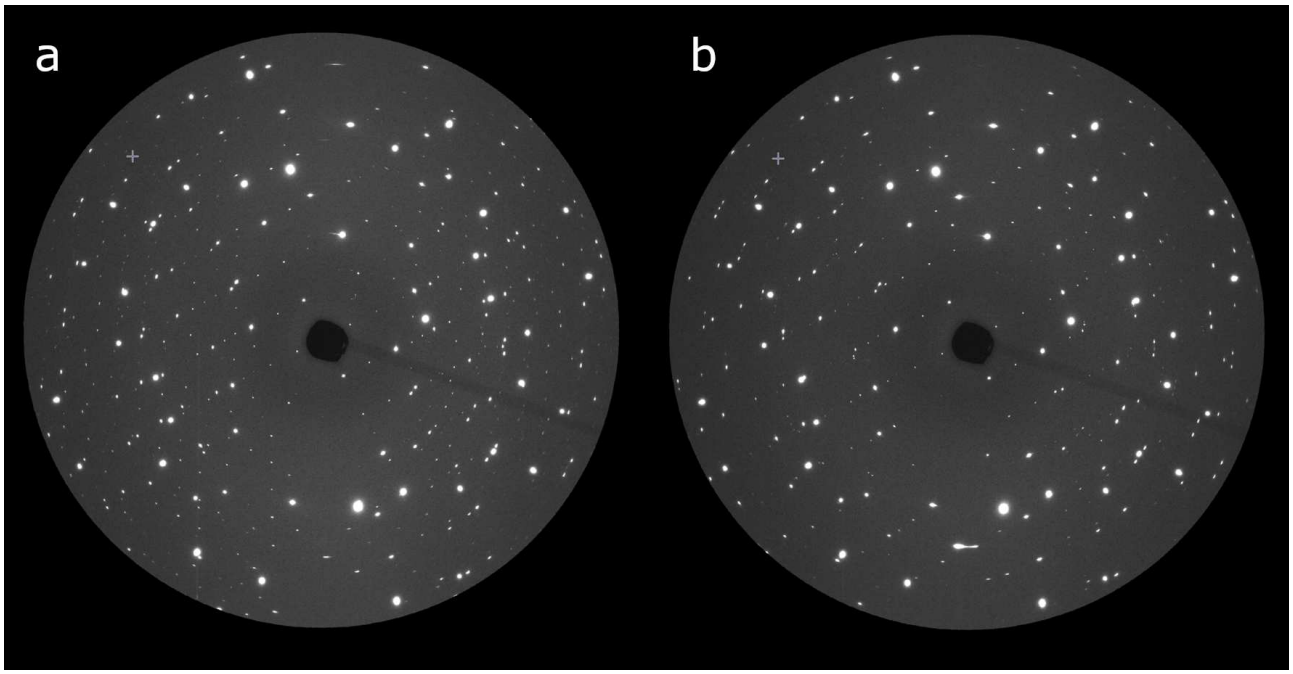

FIG. S1: Raw x-ray diffraction images of $AuAgTe_4$ at 3.2 GPa (a) and 6.7 GPa (b). Each image is a summation of 4 exposures during 17° rotation (-34° to 34°)

File Name	Cell #	Beamline/Cycle	P (GPa)	Collection	Space group	Detector	λ (Å)
crys2_P11	1	13-ID-D/2019-1	0	SC	P2/c	MARCDD	0.2952
crys2_P38	1	13-ID-D/2019-1	1.4	SC	P2/c	MARCDD	0.2952
crys2_P55	1	13-ID-D/2019-1	4.6	SC	P2/c	MARCDD	0.2952
crys2_P57	1	13-ID-D/2019-1	5.7	Wide	P2/m	MARCDD	0.2952
crys2_P59	1	13-ID-D/2019-1	6.7	Wide	P2/m	MARCDD	0.2952
crys2_P62	1	13-ID-D/2019-1	7.9	Wide	P2/m	MARCDD	0.2952
crys2_P64	1	13-ID-D/2019-1	8.8	Wide	P2/m	MARCDD	0.2952
BMC	1	13-BM-C/2019-1	10.8	SC	P2/m	Pilatus 1M	0.434
S1	1	13-ID-D/2019-2	9.7	SC	P2/m	Pilatus 1M CdTe	0.2952
D7p2	1	13-ID-D/2019-2	7.2	SC	P2/m	Pilatus 1M CdTe	0.2952
D4p4	1	13-ID-D/2019-2	4.4	SC	P2/c	Pilatus 1M CdTe	0.2952
D3p4	1	13-ID-D/2019-2	3.4	SC	P2/c	Pilatus 1M CdTe	0.2952
D2p1	1	13-ID-D/2019-2	2.1	SC	P2/c	Pilatus 1M CdTe	0.2952
D0p2	1	13-ID-D/2019-2	0.2	SC	P2/c	Pilatus 1M CdTe	0.2952

TABLE S1: Experimental details of the XRD data used in the EOS fittings for the two phases LP: $P2/c$ and HP: $P2/m$. The complete list of CCDC deposition numbers is: 2218994 - 2219002, 2215501.

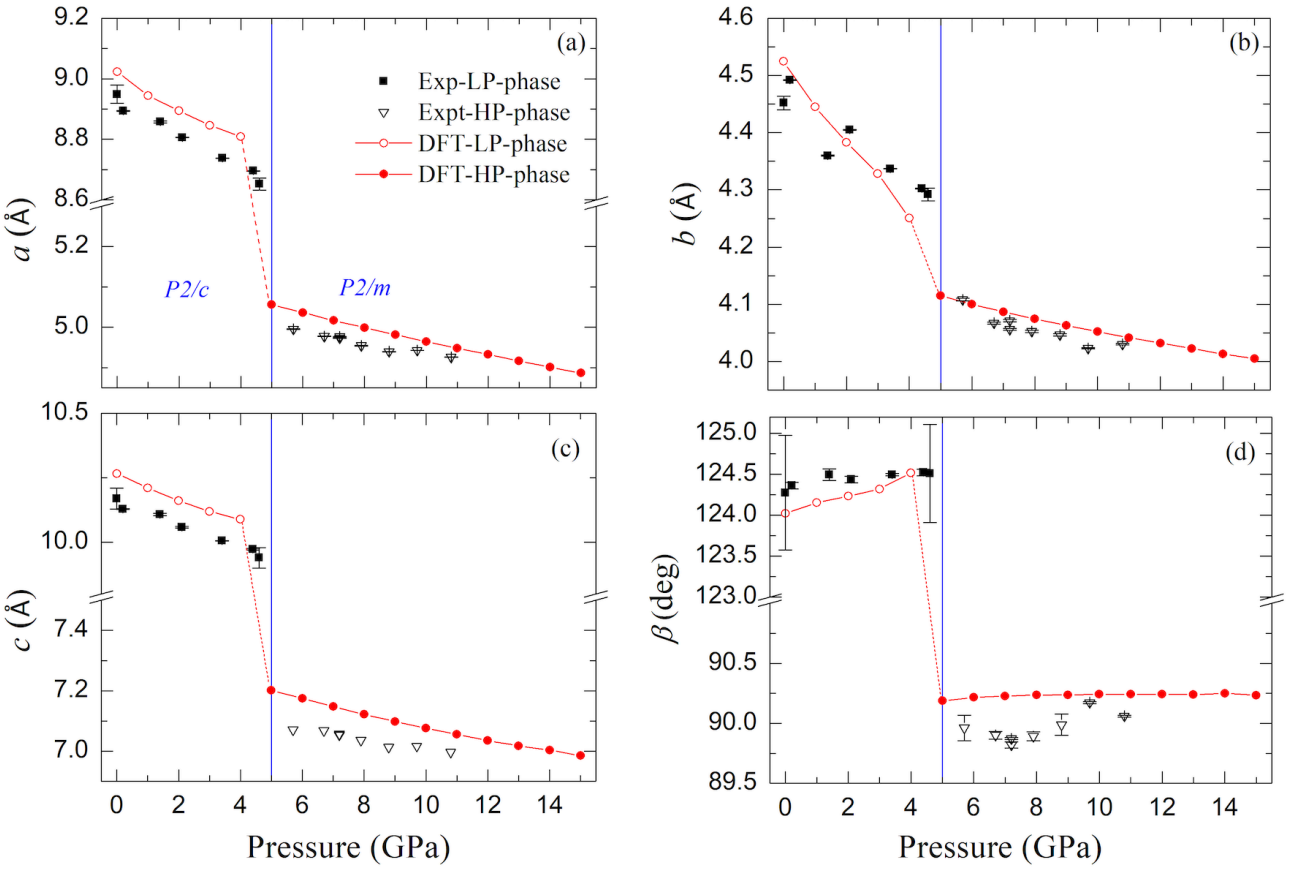

FIG. S2: Experimentally observed and calculated in DFT (shown with lines) pressure dependence of the lattice parameters a, b, c and β angle for $P2/c$ and $P2/m$ phases of $AuAgTe_4$.

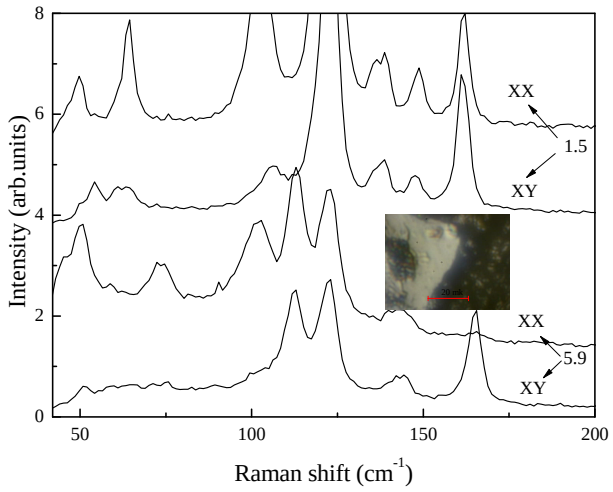

FIG. S3: Raman spectra of $AuAgTe_4$ at two pressures obtained in different polarization geometries from the single crystal fragment of which is shown in the inset.

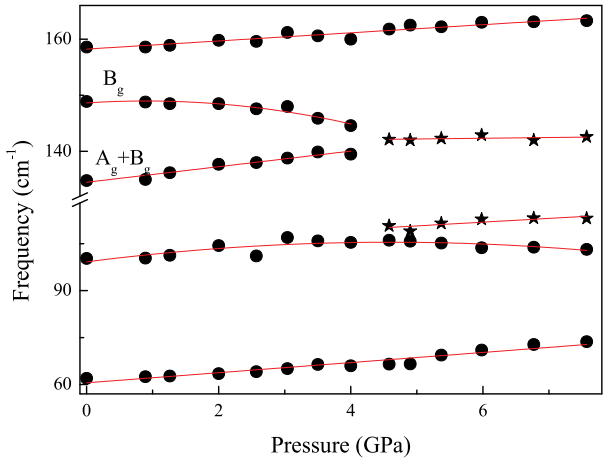

FIG. S4: Pressure dependencies of some Raman line frequencies in $AuAgTe_4$. New lines after transition are shown by stars.

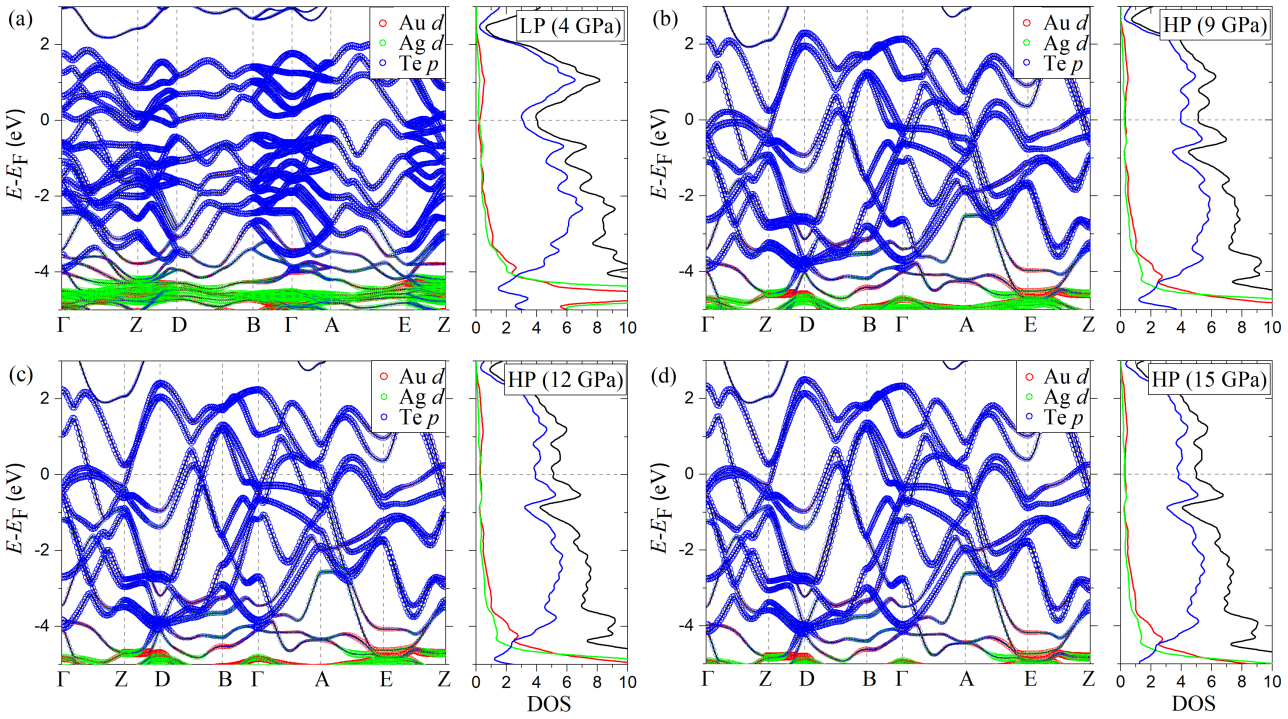

FIG. S5: Calculated band structure and DOS (states/eV/f.u.) of the LP phase of $AuAgTe_4$ at (a) 4 GPa and the HP phase at (b) 9, (c) 12, and (d) 15 GPa. The size of the symbols is proportional to the contribution of each orbital character. The solid black line in the DOS panel represents the total DOS and the red, green, and blue lines are the contributions to the DOS from the Au, Ag, and Te atoms, respectively.

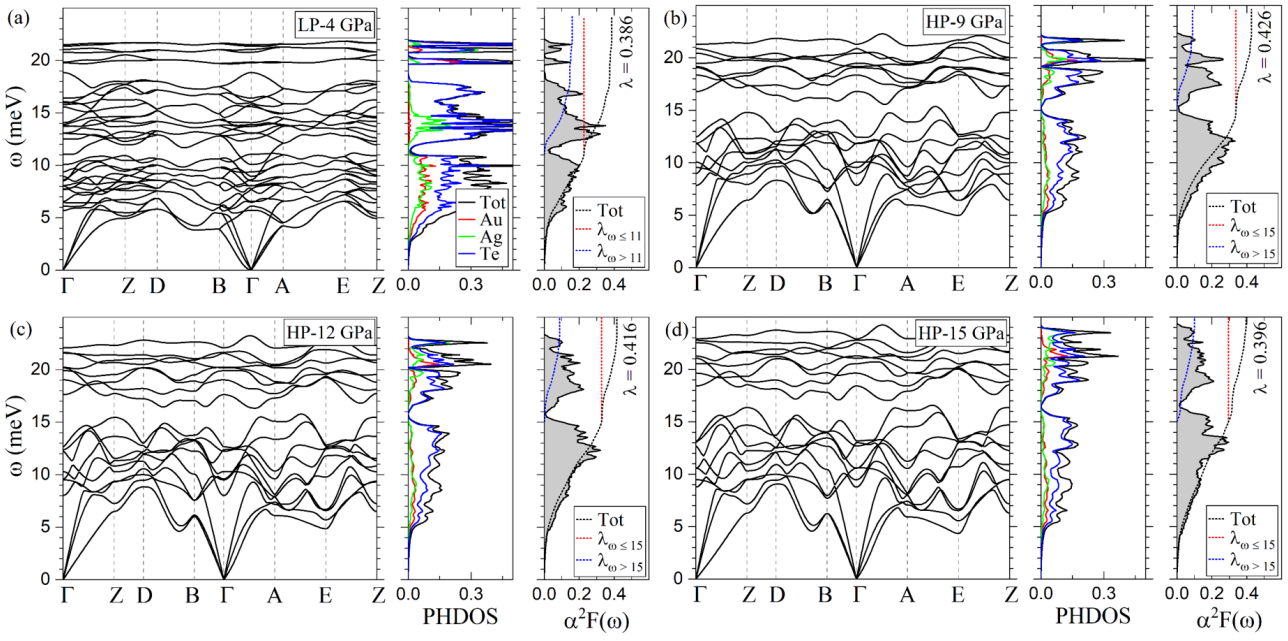

FIG. S6: Calculated phonon dispersion, PHDOS, and Eliashberg spectral function $\alpha^2F(\omega)$ of the LP phase of $AuAgTe_4$ at (a) 4 GPa and the HP phase at (b) 9, (c) 12, and (d) 15 GPa.

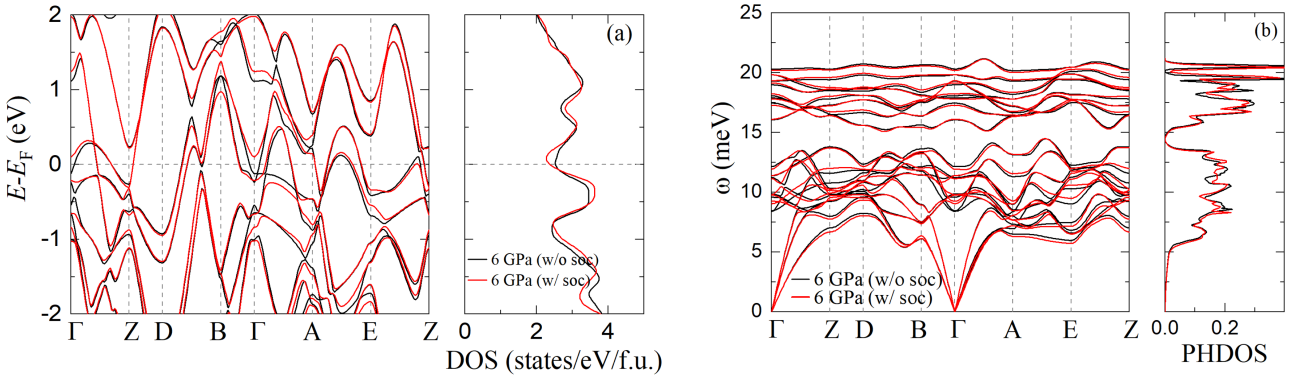

FIG. S7: Calculated (a) band structure and DOS (states/eV/f.u.), and (b) phonon dispersion and PHDOS of the HP phase of $AuAgTe_4$ at 6 GPa with (red) and without (black) spin-orbit coupling.

Pressure, GPa	0.0001	1.4	4.6	10.8	9.7 (D)	7.2 (D)	4.4 (D)	3.4 (D)	2.1 (D)	0.2 (D)
a (Å)	8.94(3)	8.8662	8.73(2)	4.9261(16)	4.9430(4)	4.9732(5)	8.6955(16)	8.7375(6)	8.8061(16)	8.8939(15)
b (Å)	4.481(12)	4.4465	4.292(11)	4.030(4)	4.0230(9)	4.0560(17)	4.3025(7)	4.3371(5)	4.4049(8)	4.4919(6)
c (Å)	14.68(4)	14.5362	14.26(4)	6.996(3)	7.0159(8)	7.0565(7)	14.329(3)	14.4028(11)	14.526(3)	14.684(2)
β	145.5(7)	145.456	145.3(6)	90.06(2)	90.173(8)	89.872(8)	145.01(4)	145.071(13)	145.17(4)	145.29(4)
V (Å^3)	333(6)	324.952	304(5)	138.89(16)	139.52(4)	142.34(6)	307.4(3)	312.50(11)	321.9(3)	334.0(3)
Reflections collected	549	627	588	354	458	456	1000	857	1057	937
Independent reflections	207	204	198	354	267	247	440	448	492	571
Independent reflections $[I>3\sigma(I)]$	297	322	302	228	256	263	577	495	601	541
Refined parameters	30	30	30	18	21	21	30	30	30	30
$R_{int}(F^2)$	0.061	0.1559	0.132	0.0320	0.001	0.0063	0.004	0.0052	0.0041	0.0055
$R(\sigma)$	0.0477	0.0585	0.0478	0.0865	0.0021	0.005	0.005	0.0057	0.0056	0.0067
$R_1[I>3\sigma(I)]$	0.0781	0.0775	0.0807	0.1105	0.0795	0.0707	0.0455	0.0440	0.0426	0.0401
$wR_2[I>3\sigma(I)]$	0.0944	0.0838	0.0892	0.2783	0.0824	0.0868	0.0579	0.0587	0.0567	0.0534
R_1	0.0868	0.1086	0.1012	0.1538	0.0798	0.0716	0.0489	0.0444	0.0459	0.0406
wR_2	0.0959	0.0949	0.0954	0.3261	0.0825	0.0878	0.0595	0.0588	0.0583	0.0535
Goodness of fit on F^2	2.33	1.87	1.97	1.157	3.77	3.54	3.76	4.03	3.69	3.59

TABLE S2: Details of the crystal structure refinements for $AuAgTe_4$ at high pressures

Au_01	Au
x	0.0
y	0.0
z	0.0
U_{11}, Å^2	0.0122(15)
U_{22}, Å^2	0.007(6)
U_{33}, Å^2	0.0106(13)
U_{23}, Å^2	0.0
U_{13}, Å^2	0.0029(12)
U_{12}, Å^2	0.0
Ag_02	Ag
x	0.0
y	0.5
z	0.5
U, Å^2	0.001(1)
Te_03	Te
x	-0.2911(10)
y	0.500000
z	-0.1650(5)
U_{11}, Å^2	0.0129(18)
U_{22}, Å^2	0.005(9)
U_{33}, Å^2	0.0124(19)
U_{23}, Å^2	0.0
U_{13}, Å^2	0.0036(16)
U_{12}, Å^2	0.0
Te_04	Te
x	-0.2978(10)
y	0.0
z	0.3305(5)
U_{11}, Å^2	0.0140(19)
U_{22}, Å^2	0.022(9)
U_{33}, Å^2	0.0113(18)
U_{23}, Å^2	0.0
U_{13}, Å^2	0.0023(17)
U_{12}, Å^2	0.0

TABLE S3: Structural data for the high-pressure phase of $AuAgTe_4$ at 10.8 GPa

[1] E. Sterer, M. P. Pasternak, and R. D. Taylor, Rev. Sci. Instrum. **61**, 1117 (1990), URL https://doi.org/10.1063/1.1141433.

[2] H. K. Mao, J.-A. Xu, and P. M. Bell, J. Geophys. Res. Solid Earth **91**, 4673 (1986), URL https://doi.org/10.1029/JB091iB05p04673.

[3] C. Prescher and V. B. Prakapenka, High Press. Res. **35**, 223 (2015), URL https://doi.org/10.1080/08957959.2015.1059835.

[4] Y. Fei, A. Ricolleau, M. Frank, K. Mibe, G. Shen, and V. Prakapenka, Proc. Natl. Acad. Sci. **104**, 9182 (2007), URL https://doi.org/10.1073/pnas.0609013104.

[5] I. Kantor, V. Prakapenka, A. Kantor, P. Dera, A. Kurnosov, S. Sinogeikin, N. Dubrovinskaia, and L. Dubrovinsky, Rev. Sci. Instrum. **83**, 125102 (2012), URL https://doi.org/10.1063/1.4768541.

[6] O. D. Rigaku, *CrysAlis PRO. Rigaku Oxford Diffraction, Rigaku Corporation* (2019).

[7] V. Petříček, M. Dušek, and L. Palatinus, Zeitschrift für Kristallographie-Crystalline Materials **229**, 345 (2014), URL https://doi.org/10.1515/zkri-2014-1737.

[8] V. Petříček, L. Palatinus, J. Plášil, and M. Dušek, Zeitschrift für Kristallographie - Crystalline Materials (2023), URL https://doi.org/10.1515/zkri-2023-0005.

[9] A. P. Hammersley *et al.*, European synchrotron radiation facility internal report ESRF97HA02T **68**, 58 (1997).

[10] A. P. Hammersley, S. O. Svensson, M. Hanfland, A. N. Fitch, and D. Hausermann, Int. J. High Press. Res. **14**, 235 (1996), URL https://doi.org/10.1080/08957959608201408.

[11] J. Gonzalez-Platas, M. Alvaro, F. Nestola, and R. Angel, J. Appl. Crystallogr. **49**, 1377 (2016), URL https://doi.org/10.1107/S1600576716008050.

[12] D. Zhang, P. K. Dera, P. J. Eng, J. E. Stubbs, J. S. Zhang, V. B. Prakapenka, and M. L. Rivers, J. Vis. Exp. p. e54660 (2017), URL https://dx.doi.org/10.3791/54660.

[13] O. V. Dolomanov, L. J. Bourhis, R. J. Gildea, J. A. K. Howard, and H. Puschmann, J. Appl. Crystallogr. **42**, 339 (2009), URL https://doi.org/10.1107/S0021889808042726.

[14] D. A. Zamyatin, E. A. Pankrushina, S. V. Streltsov, and Y. S. Ponosov, Inorganics **11** (2023), ISSN 2304-6740, URL https://www.mdpi.com/2304-6740/11/3/99.

[15] P. Giannozzi, O. Andreussi, T. Brumme, O. Bunau, M. B. Nardelli, M. Calandra, R. Car, C. Cavazzoni, D. Ceresoli, and M. Cococcioni *et.al*, J. Phys: Condens. Matter **29**, 465901 (2017), URL https://iopscience.iop.org/article/10.1088/1361-648X/aa8f79/meta.

[16] D. R. Hamann, Phys. Rev. B **88**, 085117 (2013), URL https://doi.org/10.1103/PhysRevB.88.085117.

[17] J. P. Perdew, K. Burke, and M. Ernzerhof, Phys. Rev. Lett. **77**, 3865 (1996), URL https://journals.aps.org/prl/abstract/10.1103/PhysRevLett.77.3865.

[18] M. Methfessel and A. T. Paxton, Phys. Rev. B **40**, 3616 (1989), URL https://journals.aps.org/prb/abstract/10.1103/PhysRevB.40.3616.

[19] H. J. Monkhorst and J. D. Pack, Phys. Rev. B **13**, 5188 (1976), URL https://journals.aps.org/prb/abstract/10.1103/PhysRevB.13.5188.

[20] S. Baroni, S. De Gironcoli, A. Dal Corso, and P. Giannozzi, Rev. Mod. Phys. **73**, 515 (2001), URL https://journals.aps.org/rmp/abstract/10.1103/RevModPhys.73.515.

[21] F. Giustino, M. L. Cohen, and S. G. Louie, Phys. Rev. B **76**, 165108 (2007), URL https://journals.aps.org/prb/abstract/10.1103/PhysRevB.76.165108.

[22] S. Poncé, E. R. Margine, C. Verdi, and F. Giustino, Comput. Phys. Commun. **209**, 116 (2016), URL https://www.sciencedirect.com/science/article/pii/S0010465516302260.

[23] E. R. Margine and F. Giustino, Phys. Rev. B **87**, 024505 (2013), URL https://journals.aps.org/prb/abstract/10.1103/PhysRevB.87.024505.

[24] N. Marzari, A. A. Mostofi, J. R. Yates, I. Souza, and D. Vanderbilt, Rev. Mod. Phys. **84**, 1419 (2012), URL https://journals.aps.org/rmp/abstract/10.1103/RevModPhys.84.1419.

[25] G. Pizzi, V. Vitale, R. Arita, S. Blügel, F. Freimuth, G. Géranton, M. Gibertini, D. Gresch, C. Johnson, and T. Koretsune *et.al*, J. Phys: Condens. Matter **32**, 165902 (2020), URL https://iopscience.iop.org/article/10.1088/1361-648X/ab51ff?hootPostID=8865030f3411ebd77f127a8addfbbdce.

[26] H. Shinaoka, J. Otsuki, M. Ohzeki, and K. Yoshimi, Phys. Rev. B **96**, 035147 (2017), URL https://doi.org/10.1103/PhysRevB.96.035147.

[27] J. Li, M. Wallerberger, N. Chikano, C.-N. Yeh, E. Gull, and H. Shinaoka, Phys. Rev. B **101**, 035144 (2020), URL https://doi.org/10.1103/PhysRevB.101.035144.

[28] M. Wallerberger, S. Badr, S. Hoshino, S. Huber, F. Kakizawa, T. Koretsune, Y. Nagai, K. Nogaki, T. Nomoto, H. Mori, et al., SoftwareX **21**, 101266 (2023), URL https://doi.org/10.1016/j.softx.2022.101266.